A Power-Domain NOMA Inspired Overlay Spectrum Sharing Scheme

Md. Fazlul Kader, Senior Member, IEEE *†

November 6, 2018

Abstract

Non-orthogonal multiple access (NOMA) and cooperative spectrum sharing (CSS) are integrated into this work to enhance both spectrum efficiency and utilization. An overlay spectrum sharing is proposed by exploiting NOMA in coordinated direct and relay transmission (CDRT) (termed as CSS-NOMA-CDRT). In CSS-NOMA-CDRT, a primary strong NOMA user is directly served by primary transmitter (PT), whereas a primary NOMA weak user needs the assistance of a relay to communicate with PT. Instead of using a dedicated relay, a secondary transmitter (ST) acts as a relay to forward the primary symbol to NOMA weak user and ST transmits own symbol to its receiver at the same time. The performance of the proposed CSS-NOMA-CDRT is evaluated along with closed-form solutions, in terms of ergodic sum capacity and outage probability. Through the analytical and Monte Carlo simulation results, it is demonstrated that CSS-NOMA-CDRT can obtain remarkable capacity gain as compared to the conventional NOMA-based CDRT.

Keywords Coordinated direct and relay transmission, ergodic sum capacity, non-orthogonal multiple access, outage probability, cooperative spectrum sharing.

1 Introduction

In order to deal with the various requirements of the next generation wireless networks, several candidate technologies are identified [1]. However, it may not be possible for a single technology to satisfy the performance requirements of 5G and beyond. Therefore, multiple technologies are required to be integrated [2]. Among the various candidate technologies of 5G and beyond, cognitive radio (CR) spectrum sharing and non-orthogonal multiple access (NOMA) are the two

*Manuscript received XXX, XX, 2018; revised XXX, XX, 2018.

†Md. Fazlul Kader is with the Department of Electrical and Electronic Engineering, University of Chittagong, Chittagong-4331, Bangladesh (email: f.kader@cu.ac.bd).

key techniques. The principal idea of NOMA is to exploit multiplexing in power domain to share same code/frequency/time, in attempts to significantly improve system capacity and serve massive numbers of users [3, 4]. Moreover, exploiting cooperative diversity with NOMA can further enhance system capacity and reliability [5, 6, 7].

The exponential growth of mobile traffic, quick proliferation of internet of things and high-rate data communication services may result in spectrum scarcity problem. However, this artificial scarcity of the spectrum is not because of any physical shortage of spectrum. Instead, it is largely due to inefficient fixed frequency allocations. CR is a promising and exciting technology which can tackle, or at least partially address this spectrum scarcity problem in the next generation wireless networks [8, 9]. In CR spectrum sharing, secondary or unlicensed users share the same spectrum band with primary or licensed users to enhance spectral utilization. Furthermore, integration of NOMA with spectrum sharing can enhance both spectrum efficiency and utilization [10-20], which is the main focus of this paper.

In [12], it was first identified that NOMA can be thought as a special case of a cognitive radio network (CRN), where a user experiencing better channel condition, reckoned as a secondary user (SU), may coexist at the same frequency band with a user experiencing poor channel condition, reckoned as a primary user (PU). The application of NOMA in cooperative spectrum sharing (CSS) can be broadly classified as NOMA-based underlay CSS [13-16], NOMA-based overlay CSS [17-19], and NOMA-based hybrid CSS [20].

A NOMA scheme to large-scale underlay CRNs with randomly deployed users was studied in [13]. The outage probability (OP) of the proposed protocol was assessed by stochastic geometry tools. An underlay CR network was investigated in [14], where NOMA transmission protocol was followed by two users in the secondary network (SN). It was shown that better sum rate and outage performance achieved by [14] as compared to [13] and orthogonal multiple access scheme. In [15], a power-domain NOMA inspired cooperative CRN was studied, where a decode-and-forward (DF) relay was employed to assist the simultaneous communication between a secondary transmitter (ST) and two SUs. Moreover, transmit power assigned by ST for each SU is inversely proportional to the channel gain of the corresponding link. In an underlay CRN scenario, [16] studied a cooperative NOMA scheme, where a SU having strong channel condition acted as a relay to help another SU having poor channel condition in the presence of a primary network (PN). However, the interference from PUs and bad transmission performance of SUs because of the strict power constraints imposed on secondary users are the major problem in underlay approaches.

An overlay CSS protocol using NOMA with space-time block coding can outperform the conventional superposition coding based protocol in terms of ergodic capacity (EC) and OP [17]. Basically, NOMA transmission policy was applied in phase-2, where ST (acting as a relay for PN) assigned less power to SU experiencing better channel condition and more power to PU experiencing worse channel condition. By exploiting NOMA signaling in phase-2, a CSS scheme was proposed in [18] to evaluate the performance for PN and SN in terms of system throughput and OP. By considering the relative position from the transmitter, either PU or SU can perform successive interference cancellation (SIC) in NOMA-based spectrum sharing protocol [19, 20]. In [19], a CSS scheme was investigated, where a ST was employed to assist the primary transmission. In exchange of cooperation, ST was able to transmit simultaneously with PU at the same frequency band by exploiting NOMA transmission policy. The performance improvement of a hybrid CSS protocol as compared to the traditional overlay/underlay models was demonstrated in [20], in terms of OP and ergodic sum capacity (ESC). The hybrid model jointly considered NOMA-based overlay and underlay models, under a multi-constraint and multi-relay scenario.

Exploiting NOMA in coordinated direct and relay transmission (CDRT) can be another crucial strategy for future wireless networks to enhance spectral efficiency [21]. The performance of [21] is evaluated in terms of ESC and OP under perfect SIC (pSIC). It was shown that NOMA in CDRT (NOMA-CDRT) can achieve notable capacity gain than NOMA in non-CDRT. However, [21] did not consider any spectrum sharing scenario. Therefore, a NOMA-based overlay spectrum sharing protocol for downlink transmission (termed as CSS-NOMA-CDRT) is proposed in this paper to further enhance system capacity and better spectrum utilization, where NOMA and spectrum sharing are integrated for CDRT. The primary contributions of this work are summarized as follows.

1. A two-phase CSS protocol is proposed by taking into account NOMA transmission policy in both phases over independent Rayleigh fading channels.

2. The analytical derivations of ESC and OP are provided under both pSIC and imperfect SIC (ipSIC), whereas [21]considered only pSIC.

3. The performance improvement of the proposed CSS-NOMA-CDRT over [21] is authenticated through simulation and analysis. Moreover, the correctness of analytical resutls are validated by Monte Carlo simulation.

4. We have considered a more general scenario as compared to [21]. The performance of the proposed CSS-NOMA-CDRT is evaluated for two different cases such as i) case-1 (C1)- successful decoding at relay and ii) case-2 (C2)- unsuccessful decoding at relay. Contrarily, [21] considered only C1.

The rest of this paper is organized as follows. The detailed description of the proposed CSS-NOMA-CDRT is provided in Section II along with signal-to-noise-plus-interference ratio (SNIR) formulation. The performance of CSS-NOMA-CDRT is investigated in terms of ESC and OP in Section III and V, respectively. In Section V, analytical resutls are presented via two-dimensional plots. Simulation resutls are also presented in this section to validate analytical results. At last, Section VI concludes this paper with future suggestions.

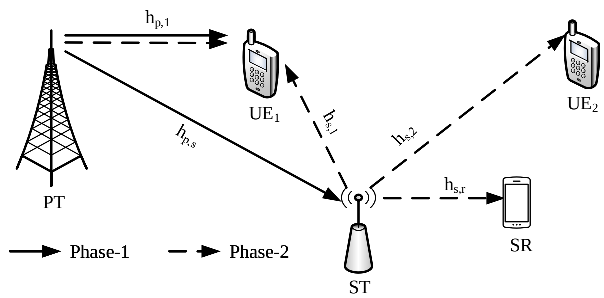

Figure 1: Proposed system model.

2 Network Model and Protocol Description

2.1 System Model

A CR spectrum sharing scenario is considered as shown in Fig. 1, wherein a SN coexist with a PN. The PN consists of a primary transmitter (PT) called as primary base station (BS) and two users UE_1 and UE_2, whereas the SN consists of a ST and a secondary receiver (SR). It is assumed that UE_1 (strong/near user) is able to communicate directly with PT, whereas the direct link between PT and UE_2 (far/weak user) does not exist or very weak due to deep fading or physical obstacles between them. Therefore, a third node called as relay is required for assisting PT to communicate with UE_2. Instead of using dedicated relay as in [21], we consider that a ST acts as a DF relay to assist primary communication. In exchange of cooperation, ST is able to simultaneously transmit own signal to SR by exploiting NOMA. Throughout the manuscript, subscripts p, s, 1, 2, and r are used to represent PT or PN, ST or SN, UE_1, UE_2, and SR, respectively.

2.2 Channel Model

The channel between any two nodes i and j is subjected to Rayleigh fading plus additive white Gaussian noise with complex channel coefficient $h_{i,j} \sim CN(0, \omega_{i,j})$, where $i, j \in$ {PT, UE_1, UE_2, ST, SR} and $i \neq j$. So, the link gain or channel gain $\alpha_{i,j} = |h_{i,j}|^2$ is exponentially distributed random variable with a mean value or scale parameter $\omega_{i,j}$. The data transmission policy along with SNIR formulation is demonstrated in the following section.

2.3 Data Transmission Policy and SNIR Model

A complete transmission in the proposed CSS-NOMA-CDRT is divided into two cooperative phases. Thus, a complete transmission requires two transmission slots t_1 and t_2.

2.3.1 Phase-1

During t_1, PT transmits a composite signal $Z_p = \sum_{i=1}^{2} \sqrt{\psi_i P_p} x_i$ following downlink NOMA principle, where x_i and ψ_i are the data symbol and power allocation coefficient, respectively related to UE$_i$. The transmit power of PT is expressed by P_p. Note that $\sum_{i=1}^{2} \psi_i = 1$ and $\psi_1 < \psi_2$. By taking into account the statistical channel state information (CSI), it is assumed that the channels are sorted as $\alpha_{p,1} > \alpha_{p,s}$ [7, 22]. Therefore, UE$_1$ performs SIC to decode x_1. The received SNIR at UE$_1$ related to symbol x_1 is given by

$$\gamma_{p,1}^{t_1} = \frac{\psi_1 \rho_p \alpha_{p,1}}{\psi_2 \rho_p \hat{\alpha}_{p,1} + 1}, \tag{1}$$

where $\rho_p \triangleq \frac{P_p}{\sigma^2}$, $\hat{\alpha}_{p,1} = |\hat{h}_{p,1}|^2$, $\hat{h}_{p,1} \sim CN(0, \zeta_1 \omega_{p,1})$, and σ^2 denotes noise variance. The symbol ζ_1 $(0 \leq \zeta_1 \leq 1)$ is a residual interference parameter considering ipSIC; $\zeta_1 = 0$ and $\zeta_1 = 1$ indicate pSIC and without SIC, respectively as a special case. Moreover, the required SNIR at UE$_1$ to decode x_2 before decoding x_1, during SIC process, is given by

$$\gamma_{p,s \to p,1}^{t_1} = \frac{\psi_2 \rho_p \alpha_{p,1}}{\psi_1 \rho_p \alpha_{p,1} + 1}. \tag{2}$$

On the other hand, ST decodes symbol x_2 assuming x_1 as noise. The received SNIR at ST is therefore given by

$$\gamma_{p,s}^{t_1} = \frac{\psi_2 \rho_p \alpha_{p,s}}{\psi_1 \rho_p \alpha_{p,s} + 1}. \tag{3}$$

2.3.2 Phase-2

There are two different cases such as C1 and C2 can happen in this phase. The detailed transmission policy in each case is provided below.

C1-Successful Decoding at ST After successful decoding of x_2 at ST, ST transmits a composite signal $Z_s = \sqrt{\psi_2 P_s} x_2 + \sqrt{\psi_r P_s} x_s$ following downlink NOMA principle, and PT transmits a new data symbol $\bar{x_1}$ to UE$_1$ with power $\psi_1^{t_2} P_p$ simultaneously with ST. The transmit power of ST is denoted by P_s and $\psi_1^{t_2}$ represents power allocation coefficient. Considering statistical CSI, it is assumed that $\alpha_{s,2} < \alpha_{s,r}$ [7,22]. Hence, SR performs SIC to decode own symbol x_s, whereas UE$_2$ decodes own symbol x_2 assuming x_s as noise. Note that $\psi_2 + \psi_r$=1 and $\psi_2 > \psi_r$; ψ_r is the power allocation coefficient related to x_s.

Because of the simultaneous transmission by PT and ST during t_2, UE$_1$ faces interference from ST. However, by exploiting the side information x_2 obtained during t_1 because of SIC procedure, UE$_1$ can cancel the interfering signal $\sqrt{\psi_2 P_s} x_2$ from the composite interfering signal Z_s. Therefore, the received SNIR at UE$_1$ is computed by

$$\gamma_{p,1}^{t_2} = \frac{\psi_1^{t_2} \rho_p \alpha_{p,1}}{\psi_r \rho_s \alpha_{s,1} + 1}. \tag{4}$$

where $\rho_s \triangleq \frac{P_s}{\sigma^2}$. In addition, the received SNIR at UE_2 is given by

$$\gamma_{s,2}^{t_2} = \frac{\psi_2 \rho_s \alpha_{s,2}}{\psi_r \rho_s \alpha_{s,2} + 1}. \tag{5}$$

Contrarily, the required SNIR at SR to decode x_2 before decoding x_s, during SIC process, is expressed by

$$\gamma_{s,2\to s,r}^{t_2} = \frac{\psi_2 \rho_s \alpha_{s,r}}{\psi_r \rho_s \alpha_{s,r} + 1}, \tag{6}$$

Moreover, the received SNIR at SR after SIC is given by

$$\gamma_{s,r}^{t_2} = \frac{\psi_r \rho_s \alpha_{s,r}}{\psi_2 \rho_s \hat{\alpha}_{s,r} + 1}, \tag{7}$$

where $\hat{\alpha}_{s,r} = |\hat{h}_{s,r}|^2$ and $\hat{h}_{s,r} \sim CN(0, \zeta_2 \omega_{s,r})$. The parameter ζ_2 expresses identical behavior to ζ_1.

C2-Unsuccessful Decoding at ST If ST is unable to decode x_2 at t_1, it will remain silent during t_2. As a result, the communication between PT and UE_2 fails and no secondary transmission also takes place during t_2. However, the interference-free communication between PT and UE_1 can occur. Therefore, the most crucial finding of this case is that the secondary transmission completely depends on the successful decoding of x_2 at ST. Then, the SNIR received at UE_1 in C2 is given by

$$\gamma_{p,1}^{t_2,C2} = \psi_1^{t_2} \rho_p \alpha_{p,1}. \tag{8}$$

3 Capacity Analysis

This section investigates EC of each user in primary and secondary systems along with closed-form expressions over independent Rayleigh fading channels. Moreover, ESC of each system and total capacity of the whole spectrum sharing network are also investigated here.

3.1 Primary system capacity

The achievable data rate of the primary system is demonstrated in this section.

3.1.1 Capacity of UE_1

Using (1) and (4), the achievable rate of UE_1 at t_1 and t_2 are respectively given by

$$C_{1,p}^{t_1} = \frac{1}{2} \log_2(1 + \gamma_{p,1}^{t_1}), \tag{9}$$

$$C_{1,p}^{t_2} = \frac{1}{2} \log_2(1 + \gamma_{p,1}^{t_2}). \tag{10}$$

Let $U = \gamma_{p,1}^{t_1} = \frac{\psi_1 \rho_p \alpha_{p,1}}{\psi_2 \rho_p \hat{\alpha}_{p,1}+1}$ and $V = \gamma_{p,1}^{t_2} = \frac{\psi_1^{t_2} \rho_p \alpha_{p,1}}{\psi_r \rho_s \alpha_{s,1}+1}$. The cumulative distribution function (CDF) of U and V can be respectively written as in [eq. (22), 23]

$$F_U(u) = 1 - \frac{\psi_1 \omega_{p,1}}{\psi_1 \omega_{p,1} + \psi_2 \zeta_1 \omega_{p,1} u} e^{-\frac{u}{\psi_1 \rho_p \omega_{p,1}}}, \tag{11}$$

$$F_V(v) = 1 - \frac{\psi_1^{t_2} \rho_p \omega_{p,1}}{\psi_1^{t_2} \rho_p \omega_{p,1} + \psi_r \rho_s \omega_{s,1} v} e^{-\frac{v}{\psi_1^{t_2} \rho_p \omega_{p,1}}}. \tag{12}$$

Let $A = \psi_1 \omega_{p,1}$, $B = \psi_2 \zeta_1 \omega_{p,1}$, $C = \psi_{p,1}^{t_2} \rho_p \omega_{p,1}$, and $D = \psi_r \rho_s \omega_{s,1}$. The exact EC related to UE_1 at t_1 and t_2 are respectively given by

$$\bar{C}_{1,p}^{t_1} = \frac{1}{2\ln 2} \int_0^\infty (1+u)^{-1} \frac{A}{A+Bu} e^{-\frac{u}{A\rho_p}} \, du, \tag{13}$$

$$\bar{C}_{1,p}^{t_2} = \frac{1}{2\ln 2} \int_0^\infty (1+v)^{-1} \frac{C}{C+Dv} e^{-\frac{v}{C}} \, dv, \tag{14}$$

where $\int_0^\infty \log_2(1+z) f_Z(z) \, dz = \frac{1}{\ln 2} \int_0^\infty \frac{1-F_Z(z)}{1+z} \, dz$ is used. The integral in (13) can be solved as

$$\begin{aligned}\bar{C}_{1,p}^{t_1} &= \frac{1}{2\ln 2} \left[\frac{A}{A-B} \left\{ \int_0^\infty (1+u)^{-1} - \int_0^\infty \frac{B}{A+Bv} \right\} e^{-\frac{u}{A\rho_p}} du \right] \\ &= \frac{1}{2\ln 2} \left[\frac{A}{A-B} \left\{ -e^{\frac{1}{A\rho_p}} \operatorname{Ei}(-\frac{1}{A\rho_p}) + e^{\frac{1}{B\rho_p}} \operatorname{Ei}(-\frac{1}{B\rho_p}) \right\} \right].\end{aligned} \tag{15}$$

where $\operatorname{Ei}(\cdot)$ represents exponential integral function [24]. It is noticed that ipSIC (i.e., $0< \zeta_1 \leq 1$) is considered to deduce (15). Hence, considering pSIC (i.e., $\zeta_1 = 0$), $U = \gamma_{p,1}^{t_1} = \frac{\psi_1 \rho_p \alpha_{p,1}}{\psi_2 \rho_p \hat{\alpha}_{p,1}+1}$ can be written as $U = \psi_1 \rho_p \alpha_{p,1}$. The CDF of U and the exact EC of UE_1 at t_1 under pSIC is therefore respectively given by

$$F_U(u) = 1 - e^{-\frac{u}{A\rho_p}}, \tag{16}$$

$$\begin{aligned}\bar{C}_{1,p}^{t_1} &= \frac{1}{2\ln 2} \int_0^\infty (1+u)^{-1} e^{-\frac{u}{A\rho_p}} \, du \\ &= -\frac{1}{2\ln 2} e^{\frac{1}{A\rho_p}} \operatorname{Ei}(-\frac{1}{A\rho_p}).\end{aligned} \tag{17}$$

Similar to (15), (14) can be derived as

$$\begin{aligned}\bar{C}_{1,p}^{t_2} &= \frac{1}{2\ln 2} \left[\frac{C}{C-D} \left\{ \int_0^\infty (1+v)^{-1} - \int_0^\infty \frac{D}{C+Dv} \right\} e^{-\frac{v}{C}} dv \right] \\ &= \frac{1}{2\ln 2} \left[\frac{C}{C-D} \left\{ -e^{\frac{1}{C}} \operatorname{Ei}(-\frac{1}{C}) + e^{\frac{1}{D}} \operatorname{Ei}(-\frac{1}{D}) \right\} \right].\end{aligned} \tag{18}$$

Moreover, using (8) and following the similar derivation to (17), the exact EC of UE$_1$ in C2 is computed as

$$\bar{C}_{1,C2}^{t_2} = -\frac{1}{2\ln 2} e^{\frac{1}{\psi_1^{t_2}\rho_p\omega_{p,1}}} \operatorname{Ei}(-\frac{1}{\psi_1^{t_2}\rho_p\omega_{p,1}}). \tag{19}$$

Now, using (15), (18) and (19), the total EC of UE$_1$ under ipSIC can be obtained as

$$\bar{C}_{1,p}^{\text{ipSIC}} = \begin{cases} (15) + (18), & \text{C1} \\ (15) + (19), & \text{C2} \end{cases} \tag{20}$$

Conversely, using (17), (18) and (19), the total EC of UE$_1$ under pSIC can be obtained as

$$\bar{C}_{1,p}^{\text{pSIC}} = \begin{cases} (17) + (18), & \text{C1} \\ (17) + (19), & \text{C2} \end{cases} \tag{21}$$

3.1.2 Capacity of UE$_2$

Using (2), (3), (5), and (6), the achievable data rate of UE$_2$ is expressed by

$$\begin{aligned} C_{2,p} &= \frac{1}{2}\log_2(1+\min(\gamma_{p,s}^{t_1}, \gamma_{p,s\to p,1}^{t_1}, \gamma_{s,2}^{t_2}, \gamma_{s,2\to s,r}^{t_2})) \\ &= \frac{1}{2}\log_2\Bigg(1+\min\bigg(\frac{\psi_2\rho_p\alpha_{p,s}}{\psi_1\rho_p\alpha_{p,s}+1}, \frac{\psi_2\rho_p\alpha_{p,1}}{\psi_1\rho_p\alpha_{p,1}+1}, \\ &\qquad \frac{\psi_2\rho_s\alpha_{s,2}}{\psi_r\rho_s\alpha_{s,2}+1}, \frac{\psi_2\rho_s\alpha_{s,r}}{\psi_r\rho_s\alpha_{s,r}+1}\bigg)\Bigg). \end{aligned} \tag{22}$$

Using [eq. (33), 7], (22) can be written as

$$C_{2,p} = \frac{1}{2}\log_2(1+\Lambda). \tag{23}$$

where $\Lambda = \frac{\min(\psi_2\rho_p\alpha_{p,s}, \psi_2\rho_p\alpha_{p,1}, \psi_2\rho_s\alpha_{s,2}, \psi_2\rho_s\alpha_{s,r})}{\min(\psi_1\rho_p\alpha_{p,s}, \psi_1\rho_p\alpha_{p,1}, \psi_r\rho_s\alpha_{s,2}, \psi_r\rho_s\alpha_{s,r})+1}$. Since it is assumed that $P_p = P_s$ and same power allocation factor ψ_2 related to x_2 in both phases for consistency, it can be chosen that ψ_r=ψ_1. Thus, (23) is written as

$$\begin{aligned} C_{2,p} &= \frac{1}{2}\log_2\left(1+\frac{\min(\rho_p\alpha_{p,s}, \rho_p\alpha_{p,1}, \rho_s\alpha_{s,2}, \rho_s\alpha_{s,r})(1-\psi_1)}{\min(\rho_p\alpha_{p,s}, \rho_p\alpha_{p,1}, \rho_s\alpha_{s,2}, \rho_s\alpha_{s,r})\psi_1+1}\right) \\ &= \frac{1}{2}\log_2\Bigg(1+\frac{\min(\rho_p\alpha_{p,s}, \rho_p\alpha_{p,1}, \rho_s\alpha_{s,2}, \rho_s\alpha_{s,r})}{\min(\rho_p\alpha_{p,s}, \rho_p\alpha_{p,1}, \rho_s\alpha_{s,2}, \rho_s\alpha_{s,r})\psi_1+1} \\ &\quad -\frac{\min(\rho_p\alpha_{p,s}, \rho_p\alpha_{p,1}, \rho_s\alpha_{s,2}, \rho_s\alpha_{s,r})\psi_1}{\min(\rho_p\alpha_{p,s}, \rho_p\alpha_{p,1}, \rho_s\alpha_{s,2}, \rho_s\alpha_{s,r})\psi_1+1}\Bigg) \\ &= \frac{1}{2}\log_2\left(\frac{\min(\rho_p\alpha_{p,s}, \rho_p\alpha_{p,1}, \rho_s\alpha_{s,2}, \rho_s\alpha_{s,r})+1}{\min(\rho_p\alpha_{p,s}, \rho_p\alpha_{p,1}, \rho_s\alpha_{s,2}, \rho_s\alpha_{s,r})\psi_1+1}\right), \end{aligned} \tag{24}$$

where $\psi_2 = 1 - \psi_1$ is used. Now, using $\log_a(x/y) = \log_a x - \log_a y$, (24) can be expanded as

$$C_{2,p} = \frac{1}{2}\log_2(1+\min(\rho_p\alpha_{p,s}, \rho_p\alpha_{p,1}, \rho_s\alpha_{s,2}, \rho_s\alpha_{s,r})) \\ - \frac{1}{2}\log_2(1+\min(\rho_p\alpha_{p,s}, \rho_p\alpha_{p,1}, \rho_s\alpha_{s,2}, \rho_s\alpha_{s,r})\psi_1). \quad (25)$$

Let $W = \min(\rho_p\alpha_{p,s}, \rho_p\alpha_{p,1}, \rho_s\alpha_{s,2}, \rho_s\alpha_{s,r})$ and $X = \min(\rho_p\alpha_{p,s}, \rho_p\alpha_{p,1}, \rho_s\alpha_{s,2}, \rho_s\alpha_{s,r})\psi_1$. Using the CDF of the minimum of two exponential distributed RVs, the CDFs of W and X are given by

$$F_W(w) = 1 - e^{-w(\frac{1}{\rho_p\omega_{p,s}}+\frac{1}{\rho_p\omega_{p,1}}+\frac{1}{\rho_s\omega_{s,2}}+\frac{1}{\rho_s\omega_{s,r}})}, \quad (26)$$

$$F_X(x) = 1 - e^{-x(\frac{1}{\psi_1\rho_p\omega_{p,s}}+\frac{1}{\psi_1\rho_p\omega_{p,1}}+\frac{1}{\psi_1\rho_s\omega_{s,2}}+\frac{1}{\psi_1\rho_s\omega_{s,r}})}. \quad (27)$$

Now, using (26) and (27), the exact EC of UE_2 is obtained by

$$\begin{aligned}\bar{C}_{2,p} &= \frac{1}{2\ln 2}\int_0^\infty (1+w)^{-1} e^{-w\beta}\, dw \\ &- \frac{1}{2\ln 2}\int_0^\infty (1+x)^{-1} e^{-x\delta}\, dx \\ &= \frac{1}{2\ln 2}\left\{-e^{\beta}\,\text{Ei}(-\beta) + e^{\delta}\,\text{Ei}(-\delta)\right\},\end{aligned} \quad (28)$$

where $\beta = \frac{1}{\rho_p\omega_{p,s}} + \frac{1}{\rho_p\omega_{p,1}} + \frac{1}{\rho_s\omega_{s,2}} + \frac{1}{\rho_s\omega_{s,r}}$, $\delta = \frac{1}{\psi_1\rho_p\omega_{p,s}} + \frac{1}{\psi_1\rho_p\omega_{p,1}} + \frac{1}{\psi_1\rho_s\omega_{s,2}} + \frac{1}{\psi_1\rho_s\omega_{s,r}}$, and $\int_0^\infty \log_2(1+z) f_Z(z)\, dz = \frac{1}{\ln 2}\int_0^\infty \frac{1-F_Z(z)}{1+z}\, dz$ is used.

3.1.3 Sum capacity of PN

Using (20) and (28), the total EC of PN under ipSIC is obtained as

$$\bar{C}_{\text{PN}}^{\text{ipSIC}} = \begin{cases} (15)+(18)+(28), & \text{C1} \\ (15)+(19), & \text{C2} \end{cases} \quad (29)$$

Conversely, using (21), and (28), the total EC of PN under pSIC is obtained as

$$\bar{C}_{\text{PN}}^{\text{pSIC}} = \begin{cases} (17)+(18)+(28), & \text{C1} \\ (17)+(19), & \text{C2} \end{cases} \quad (30)$$

3.2 Capacity of SN

Using (7), the achievable data rate of SN is written by

$$C_{\text{SN}} = \frac{1}{2}\log_2(1+\gamma_{s,r}^{t_2}). \quad (31)$$

Let $Y = \gamma_{s,r}^{t_2} = \frac{\psi_r \rho_s \alpha_{s,r}}{\psi_2 \rho_s \hat{\alpha}_{s,r}+1} = \frac{\psi_1 \rho_s \alpha_{s,r}}{\psi_2 \rho_s \hat{\alpha}_{s,r}+1}$. Similar to (11), The CDF of Y is written by

$$F_Y(y) = 1 - \frac{E}{E+Fy} e^{-\frac{y}{E\rho_s}}, \tag{32}$$

where $E = \psi_1 \omega_{s,r}$ and $F = \psi_2 \zeta_2 \omega_{s,r}$. The exact EC of SN is therefore given by

$$\bar{C}_{\mathrm{SN}} = \frac{1}{2\ln 2} \int_0^\infty (1+y)^{-1} \frac{E}{E+Fy} e^{-\frac{y}{E\rho_s}} \, dy. \tag{33}$$

Similar to (15), (33) can be derived as

$$\begin{aligned}\bar{C}_{\mathrm{SN}} &= \frac{1}{2\ln 2}\left[\frac{E}{E-F}\left\{\int_0^\infty (1+y)^{-1} - \int_0^\infty \frac{F}{E+Fy}\right\} e^{-\frac{y}{E\rho_s}} dy\right] \\ &= \frac{1}{2\ln 2}\left[\frac{E}{E-F}\left\{-e^{\frac{1}{E\rho_s}} \mathrm{Ei}(-\frac{1}{E\rho_s}) + e^{\frac{1}{F\rho_s}} \mathrm{Ei}(-\frac{1}{F\rho_s})\right\}\right].\end{aligned} \tag{34}$$

It is observed that ipSIC (i.e., $0< \zeta_2 \leq 1$) is thought to deduce (34). Hence, considering pSIC (i.e., $\zeta_2 = 0$), $Y = \gamma_{s,r}^{t_2} = \frac{\psi_1 \rho_s \alpha_{s,r}}{\psi_2 \rho_s \hat{\alpha}_{s,r}+1}$ can be written as $Y = \psi_1 \rho_s \alpha_{s,r}$. The exact EC of SN under pSIC is therefore given by

$$\bar{C}_{\mathrm{SN}} = -\frac{1}{2\ln 2} e^{\frac{1}{E\rho_s}} \mathrm{Ei}(-\frac{1}{E\rho_s}). \tag{35}$$

3.3 Total system capacity

Using (29) and (34), the ESC of the proposed spectrum sharing network under ipSIC is obtained as

$$\bar{C}_{\mathrm{CSS}}^{\mathrm{ipSIC}} = \begin{cases} (15) + (18) + (28) + (34), & \mathrm{C1} \\ (15) + (19), & \mathrm{C2} \end{cases} \tag{36}$$

Conversely, using (30), and (35), the ESC of the proposed spectrum sharing network under pSIC is obtained as

$$\bar{C}_{\mathrm{CSS}}^{\mathrm{pSIC}} = \begin{cases} (17) + (18) + (28) + (35), & \mathrm{C1} \\ (17) + (19), & \mathrm{C2} \end{cases} \tag{37}$$

4 Outage probability analysis

Analytical expression of OP for each user in PN and SN is provided over independent Rayleigh fading channels, in this section. Let R_{p_1}, R_{p_2}, and R_s are the predefined target rate threshold of UE_1, UE_2, and SU respectively, according to the required quality of service.

4.1 Outage probability of PN

4.1.1 Outage probability of UE$_1$

The OP of UE$_1$ at t_1 under ipSIC is given by

$$\begin{aligned} P_{1,p}^{t_1,\text{ipSIC}} &= 1 - P_r\{(\gamma_{p,1}^{t_1} > R_{p_1}^{th}) \cap (\gamma_{p,s\to p,1}^{t_1} > R_{p_2}^{th})\} \\ &= 1 - P_r(\gamma_{p,1}^{t_1} > R_{p_1}^{th}) P_r(\gamma_{p,s\to p,1}^{t_1} > R_{p_2}^{th}) \\ &= 1 - \frac{\psi_1\omega_{p,1}}{\psi_1\omega_{p,1} + \psi_2\zeta_1\omega_{p,1}R_{p_1}^{th}} e^{-\frac{R_{p_1}^{th}}{\psi_1\rho_p\omega_{p,1}} - \frac{R_{p_1}^{th}}{\omega_{p,1}\rho_p(\psi_2 - \psi_1 R_{p_1}^{th})}}, \end{aligned} \tag{38}$$

where $R_{p_1}^{th} = 2^{2R_{p_1}} - 1$, $R_{p_2}^{th} = 2^{2R_{p_2}} - 1$ and $\frac{R_{p_2}^{th}}{R_{p_2}^{th}+1} < \psi_2 < 1$. On the other hand, the OP of UE$_1$ at t_1 under pSIC (i.e., $\zeta_1 = 0$) is expressed as

$$P_{1,p}^{t_1,\text{pSIC}} = 1 - e^{-\frac{R_{p_1}^{th}}{\psi_1\rho_p\omega_{p,1}} - \frac{R_{p_1}^{th}}{\omega_{p,1}\rho_p(\psi_2 - \psi_1 R_{p_1}^{th})}}, \tag{39}$$

Moreover, the OP of UE$_1$ at t_2 in C1 and C2 is respectively given by

$$\begin{aligned} P_{1,p}^{t_2,\text{C1}} &= 1 - P_r(\gamma_{p,1}^{t_2} > R_{p_1}^{th}) \\ &= 1 - \frac{\psi_1^{t_2}\rho_p\omega_{p,1}}{\psi_1^{t_2}\rho_p\omega_{p,1} + \psi_1\rho_s\omega_{s,1}R_{p_1}^{th}} e^{-\frac{R_{p_1}^{th}}{\psi_1^{t_2}\rho_p\omega_{p,1}}}, \end{aligned} \tag{40}$$

$$P_{1,p}^{t_2,\text{C2}} = 1 - P_r(\gamma_{p,1}^{t_2,\text{C2}} > R_{p_1}^{th}) = 1 - e^{-\frac{R_{p_1}^{th}}{\psi_1^{t_2}\rho_p\omega_{p,1}}}. \tag{41}$$

4.1.2 Outage probability of UE$_2$

The OP of UE$_2$ is given by

$$\begin{aligned} P_{2,p} &= 1 - P_r(\gamma_{p,s}^{t_1} > R_{p_2}^{th}) P_r(\gamma_{s,2}^{t_2} > R_{p_2}^{th}) \\ &= 1 - e^{-\frac{R_{p_2}^{th}}{\omega_{p,s}\rho_p(\psi_2 - \psi_1 R_{p_2}^{th})} - \frac{R_{p_2}^{th}}{\omega_{s,2}\rho_s(\psi_2 - \psi_1 R_{p_2}^{th})}}. \end{aligned} \tag{42}$$

4.2 Outage probability of SN

It should be mentioned that the secondary transmission wholly depends on the successful decoding of x_2 at ST during t_1. If ST is unable to decode x_2, then SN will be in outage. Hence, the OP of SN is given by

$$\begin{aligned} P_s &= 1 - P_r(\gamma_{s,r}^{t_2} > R_s^{th}) P_r(\gamma_{p,s}^{t_1} > R_{p_2}^{th}) P_r(\gamma_{s,2\to s,r}^{t_2} > R_{p_2}^{th}) \\ &= 1 - \frac{\psi_1\omega_{s,r}}{\psi_1\omega_{s,r} + \psi_2\zeta_2\omega_{s,r}R_s^{th}} \\ &\times e^{-\frac{R_s^{th}}{\psi_1\rho_s\omega_{s,r}} - \frac{R_{p_2}^{th}}{\omega_{p,s}\rho_p(\psi_2 - \psi_1 R_{p_2}^{th})} - \frac{R_{p_2}^{th}}{\omega_{s,r}\rho_s(\psi_2 - \psi_1 R_{p_2}^{th})}}, \end{aligned} \tag{43}$$

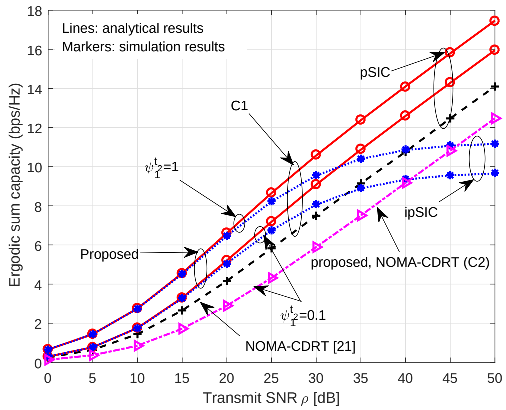

Figure 2: ESC comparison between CSS-NOMA-CDRT and CDRT-NOMA [21] w.r.t transmit SNR ρ showing the impact of varying $\psi_1^{t_2}$. ψ_1=0.1, ψ_2=0.9, $\omega_{p,1} = \omega_{s,r}$=1, $\omega_{p,s} = \omega_{s,2}$=0.5, $\omega_{s,1}$=0.1, and $\zeta = 0.04^2$.

where $R_s^{th} = 2^{2R_s} - 1$. On the other hand, the OP of SN under pSIC (i.e., ζ_2=0) is expressed by

$$P_s = 1 - e^{-\frac{R_s^{th}}{\psi_1 \rho_s \omega_{s,r}} - \frac{R_{p_2}^{th}}{\omega_{p,s} \rho_p (\psi_2 - \psi_1 R_{p_2}^{th})} - \frac{R_{p_2}^{th}}{\omega_{s,r} \rho_s (\psi_2 - \psi_1 R_{p_2}^{th})}}. \tag{44}$$

5 Numerical results

The analytical (Anl.) and simulation (Sim.) results are presented in this section to evaluate performance of the proposed CSS-NOMA-CDRT, in terms of ESC/EC and OP. The simulation results for NOMA-CDRT [21] are also plotted for comparison purpose. Throughout the simulation, it is considered that R_{p_1}= R_{p_2}= R_s=R_t, ψ_1=0.1, ψ_2=0.9, $\psi_1^{t_2}$=1, $\omega_{p,1} = \omega_{s,r}$=1, $\omega_{p,s} = \omega_{s,2}$=0.5, $\omega_{s,1}$=0.1, $\rho_p = \rho_s = \rho$, and $\zeta_1 = \zeta_2 = \zeta$, unless otherwise defined. It should be mentioned that fixed power allocation method as in [21] is assumed for a fair comparison. Moreover, it is shown that in each case analytical result is well verified with the simulation, which establishes the legitimacy of our analysis.

5.1 Ergodic capacity

Figs. 2 and 3 demonstrate ESC comparison between CSS-NOMA-CDRT and CDRT-NOMA [21] with respect to (w.r.t) transmit SNR ρ, where ρ varies from 0 to 50 dB. Fig. 2 depicts ESC presenting the impact of varying $\psi_1^{t_2}$, whereas Fig. 3 demonstrates ESC showing the impact of varying ζ and $\omega_{s,1}$. From both figures, it is clearly observed that CSS-NOMA-CDRT shows outstanding capacity gain than CDRT-NOMA under pSIC, whereas under ipSIC, the level of

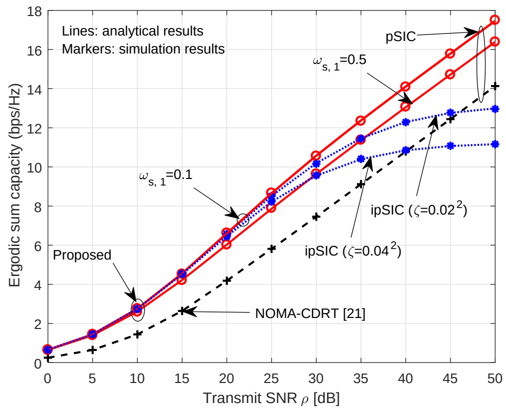

Figure 3: ESC comparison between proposed and CDRT-NOMA [21] w.r.t transmit SNR ρ showing the impact of varying ζ and $\omega_{s,1}$. ψ_1=0.1, ψ_2=0.9, $\psi_1^{t_2}$=1, $\omega_{p,1} = \omega_{s,r}$=1, and $\omega_{p,s} = \omega_{s,2}$=0.5.

residual interference ζ has a significant impact on the capacity gain, particularly at high ρ. This capacity gain is because of spectrum sharing nature of CSS-NOMA-CDRT. Moreover, ESC in C1 shows better performance than ESC in C2. Although, [21] did not consider C2, we have shown here that both protocols show similar performance in C2. This means that when ST or relay is unable to decode symbol during phase-1, it will keep silent throughout phase-2, although BS or PT can still transmit new symbol to UE_1. As a consequence, there is no transmission between BS to UE_2 in [21] as well as PT to UE_2 and ST to SR in CSS-NOMA-CDRT, resulting capacity decrease in both approaches. From Fig. 2, it is clear that if PT assigns its full power to transmit symbol in phase-2, better capacity can be achieved than the transmitting symbol with partial power allocation. From Fig. 3, it is pointed out that ESC with $\zeta = 0.02^2$ outperforms ESC with $\zeta = 0.04^2$. This is due to the fact that the lower value of ζ indicates better interference cancellation and vice versa. It is also observed that if UE_1 faces less interference from ST, higher system capacity can be obtained in CSS-NOMA-CDRT. Lastly, ESC improves with an increase in ρ, as anticipated. Note that all the figures except Figs. 2 and 6 are plotted by considering only C1.

Fig. 4 and 5 plot EC comparison between PN and SN w.r.t transmit SNR ρ and power allocation coefficient ψ_1, respectively. From both figures, it is remarked that PN achieves significantly better capacity than SN. This is because of the fact that primary transmission is possible in both phases, whereas secondary transmission is allowed only in phase-2. It is pointed out from Fig. 4 that EC with pSIC outperforms EC with ipSIC. From Fig. 5, it is seen that SN shows identical performance to UE_1 at t_1; this is because of similar parameters consideration in both protocols. Finally, it is shown that power allocation factors have a substantial impact on the performance of PN and SN.

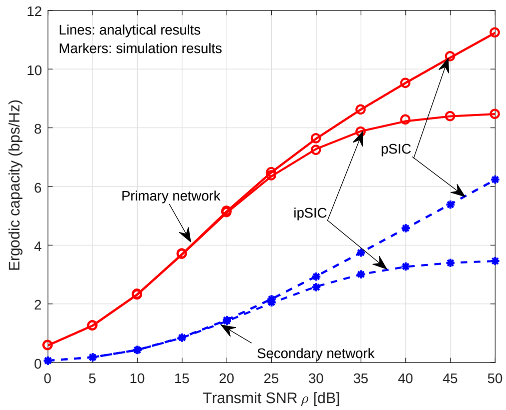

Figure 4: EC comparison between PN and SN w.r.t transmit SNR ρ. ψ_1=0.1, ψ_2=0.9, $\psi_1^{t_2}$=1, $\omega_{p,1} = \omega_{s,r}$=1, $\omega_{p,s} = \omega_{s,2}$=0.5, $\omega_{s,1}$=0.1, and $\zeta = 0.03^2$.

5.2 Outage probability

Outage behavior of the users in CSS-NOMA-CDRT is investigated in Figs. 6 and 7 w.r.t transmit SNR ρ, where ρ varies from 0 to 45 dB. Fig. 6 shows OP of each user under pSIC, whereas Fig. 7 shows OP of UE_1 at t_1 and SN to show the impact of both pSIC and ipSIC. Note that SIC is performed at UE_1 during t_1 and at SR during t_2. It is observed from Fig. 6 that UE_1 at t_2 in C2 outperforms others, with the system parameters assumed here. This is because of the fact that in C2, UE_1 can receive PT's signal without facing any interference from ST. However, system capacity degrades significantly in C2 as shown in Figs. 2 and 3. On the other hand, OP of UE_1 at t_2 in C1 decreases linearly up to a certain ρ, after that it shows a constant behavior because of facing higher interference from ST at high ρ. It is also found that UE_2 shows better performance than UE_1 at t_1 and SN. A further key observation from Fig. 6 and 7 is that SN shows slightly higher OP than UE_1 at t_1 in C1, although similar parameters are considered for both of them. The main reason is that the secondary transmission also depends on the successful decoding of primary symbol at ST during t_1. Furthermore, two cases of R_t where R_t=0.5 bps/Hz and R_t=1 bps/Hz as well as two cases of ζ, where $\zeta = 0.0.2^2$ and $\zeta = 0.04^2$, are considered for Fig. 7. It is found that OP with pSIC outperforms OP with ipSIC for any cases of ζ and R_t. It is also seen that OP with $\zeta = 0.02^2$ shows better performance than OP with $\zeta = 0.04^2$. Lastly, it is noticed that OP degrades with an increasing value of R_t, as expected.

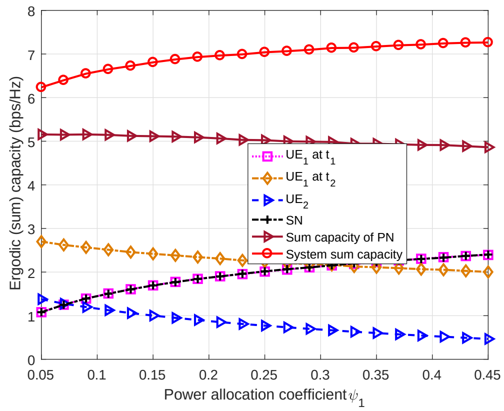

Figure 5: EC comparison between PN and SN w.r.t power allocation coefficient ψ_1 under pSIC. $\psi_1^{t_2}$=1, $\omega_{p,1} = \omega_{s,r}$=1, $\omega_{p,s} = \omega_{s,2}$=0.5, $\omega_{s,1}$=0.1, and $\rho = 20$ dB.

6 Conclusion and future works

An overlay spectrum sharing is proposed and investigated by exploiting NOMA in CDRT. The performance of the proposed CSS-NOMA-CDRT is assessed, in terms of ESC/EC and OP. The closed-form solutions of ESC/EC and OP are also provided and verified with Monte Carlo simulation. It is observed that CSS-NOMA-CDRT can obtain a notable capacity gain as compared to its counterpart, conventional NOMA-CDRT. On the performance of CSS-NOMA-CDRT and NOMA-CDRT, the impact of different system parameters are also studied. To the best of author's knowledge, this is the basic work related to CSS in NOMA-based CDRT. Therefore, this work can be extended further to be applied in multiple-input multiple-output scenario, which is subjected to future works.

References

[1] Z. Ma, Z. Zhang, Z. Ding, P. Fan, and H. Li, "Key techniques for 5G wireless communications: Network architecture, physical layer, and MAC layer perspectives," *Sci. China Info. Sci.*, vol. 58, no. 4, pp. 1–20, Apr. 2015.

[2] W. H. Chin, Z. Fan, and R. Haines, "Emerging technologies and research challenges for 5G wireless networks," *IEEE Wireless Commun.*, vol. 21, no. 2, pp. 106–112, Apr. 2014.

[3] S. M. R. Islam, N. Avazov, O. A. Dobre, and K. S. Kwak, "Power-domain non-orthogonal multiple access (NOMA) in 5G systems: Potentials and

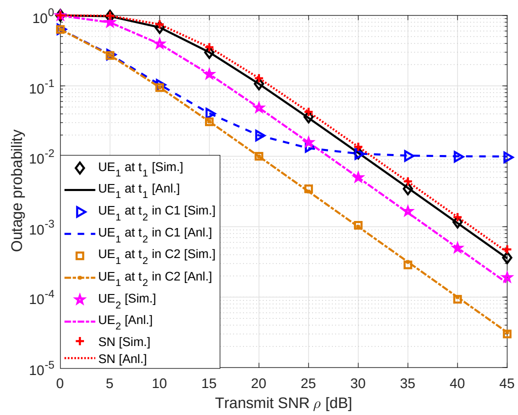

Figure 6: OP comparison between PN and SN w.r.t transmit SNR ρ under pSIC. ψ_1=0.1, ψ_2=0.9, $\psi_1^{t_2}$=1, $\omega_{p,1} = \omega_{s,r}$=1, $\omega_{p,s} = \omega_{s,2}$=0.5, $\omega_{s,1}$=0.1, and R_t=0.5 bps/Hz.

challenges," *IEEE Commun. Surveys Tuts.*, vol. 19, no. 2, pp. 721–742, Secondquarter 2017.

[4] L. Dai, B. Wang, Y. Yuan, S. Han, C. l. I, and Z. Wang, "Non-orthogonal multiple access for 5G: Solutions, challenges, opportunities, and future research trends," *IEEE Commun. Mag.*, vol. 53, no. 9, pp. 74–81, Sept. 2015.

[5] J. Kim and I. Lee, "Capacity analysis of cooperative relaying systems using non-orthogonal multiple access," *IEEE Commun. Lett.*, vol. 19, no. 11, pp. 1949–1952, Nov 2015.

[6] M. F. Kader, M. B. Shahab, and S. Y. Shin, "Exploiting non-orthogonal multiple access in cooperative relay sharing," *IEEE Commun. Lett.*, vol. 21, no. 5, pp. 1159–1162, May 2017.

[7] M. F. Kader and S. Y. Shin, "Cooperative relaying using space-time block coded non-orthogonal multiple access," *IEEE Trans. Veh. Technol.*, vol. 66, no. 7, pp. 5894–5903, Jul. 2017.

[8] X. Hong, J. Wang, C.-X. Wang, and J. Shi, "Cognitive radio in 5G: A perspective on energy-spectral efficiency trade-off," *IEEE Commun Mag.*, vol. 52, no. 7, pp. 46–53, Jul. 2014.

[9] F. Hu, B. Chen, and K. Zhu, "Full spectrum sharing in cognitive radio networks toward 5G: A survey," *IEEE Access*, vol. 6, pp. 15 754–15 776, 2018.

[10] F. Zhou, Y. Wu, Y. C. Liang, Z. Li, Y. Wang, and K. K. Wong, "State of the art, taxonomy, and open issues on cognitive radio networks with NOMA," *IEEE Wireless Commun.*, vol. 25, no. 2, pp. 100–108, Apr. 2018.

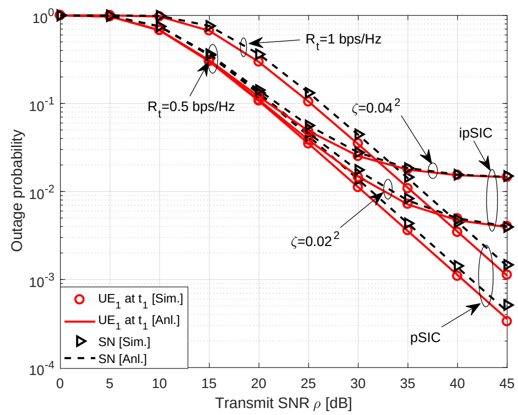

Figure 7: OP of UE_1 at t_1 and SN w.r.t transmit SNR ρ under pSIC and ipSIC. ψ_1=0.1, ψ_2=0.9, $\psi_1^{t_2}$=1, $\omega_{p,1} = \omega_{s,r}$=1, $\omega_{p,s} = \omega_{s,2}$=0.5, and $\omega_{s,1}$=0.1.

[11] L. Lv, J. Chen, Q. Ni, Z. Ding, and H. Jiang, "Cognitive non-orthogonal multiple access with cooperative relaying: A new wireless frontier for 5G spectrum sharing," *IEEE Commun. Mag*, vol. 56, no. 4, pp. 188–195, Apr. 2018.

[12] Z. Ding, P. Fan, and H. V. Poor, "Impact of user pairing on 5G nonorthogonal multiple-access downlink transmissions," *IEEE Trans. Veh. Technol.*, vol. 65, no. 8, pp. 6010–6023, Aug 2016.

[13] Y. Liu, Z. Ding, M. Elkashlan, and J. Yuan, "Nonorthogonal multiple access in large-scale underlay cognitive radio networks," *IEEE Trans. Veh. Technol.*, vol. 65, no. 12, pp. 10 152–10 157, Dec 2016.

[14] N. Zabetian, M. Baghani, and A. Mohammadi, "Rate optimization in NOMA cognitive radio networks," in *2016 8th International Symposium on Telecommunications (IST)*, Sept 2016, pp. 62–65.

[15] T. M. C. Chu and H. Zepernick, "Non-orthogonal multiple access for DF cognitive cooperative radio networks," in *2018 IEEE International Conference on Communications Workshops (ICC Workshops)*, May 2018, pp. 1–6.

[16] S. Lee, T. Q. Duong, D. B. da Costa, D. B. Ha, and S. Q. Nguyen, "Underlay cognitive radio networks with cooperative non-orthogonal multiple access," *IET Commun.*, vol. 12, no. 3, pp. 359–366, 2018.

[17] M. F. Kader and S. Y. Shin, "Cooperative spectrum sharing with space time block coding and non-orthogonal multiple access," in *2016 Eighth International Conference on Ubiquitous and Future Networks (ICUFN)*, Jul. 2016, pp. 490–494.

[18] L. Lv, Q. Ni, Z. Ding, and J. Chen, "Application of non-orthogonal multiple access in cooperative spectrum-sharing networks over Nakagami- m fading channels," *IEEE Trans. Veh. Technol.*, vol. 66, no. 6, pp. 5506–5511, Jun. 2017.

[19] M. F. Kader and S. Y. Shin, "Performance analysis of cooperative spectrum sharing using nonorthogonal multiple access," *Int J. Commun. Syst.*, vol. 31, no. 4, p. e3481, Mar. 2018.

[20] ——, "Cooperative hybrid spectrum sharing: A NOMA-based approach," *Wireless Per. Commun.*, vol. 96, no. 1, pp. 1–21, Sep. 2017.

[21] J. B. Kim and I. H. Lee, "Non-orthogonal multiple access in coordinated direct and relay transmission," *IEEE Commun. Lett.*, vol. 19, no. 11, pp. 2037–2040, Nov. 2015.

[22] Z. Wei, L. Dai, D. W. K. Ng, and J. Yuan, "Performance analysis of a hybrid downlink-uplink cooperative NOMA scheme," in *2017 IEEE 85th Vehicular Technology Conference (VTC Spring)*, June 2017, pp. 1–7.

[23] C. Zhong and Z. Zhang, "Non-orthogonal multiple access with cooperative full-duplex relaying," *IEEE Commun. Lett.*, vol. 20, no. 12, pp. 2478–2481, Dec 2016.

[24] I. S. Gradshteyn and I. M. Ryzhik, *Table of integrals, series and products 7th edn.* New York, NY, USA: Academic, 2007.

Biography Md. Fazlul Kader (S'17-M'18-SM'18) received the B.Sc. and M.Sc. degrees in computer science and engineering from the Chittagong University of Engineering and Technology, Chittagong, Bangladesh, in November 2005 and January 2014, respectively. He was awarded the Ph.D. degree from the Kumoh National Institute of Technology, Gumi, South Korea, in February 2018.

Since 2007, he has been a faculty member with the Department of Electrical and Electronic Engineering, University of Chittagong, Chittagong, Bangladesh, where he is currently an Associate Professor. He has co-authored more than 45 technical papers in international journals and conference proceedings. He is an Associate Editor of the IEEE Access. Moreover, he regularly serves as a reviewer and TPC member in many reputed journals and conferences. His major research interests include 5G, cognitive radio networks, cooperative communications, MIMO, computer networks, NOMA, spatial modulation etc.